Cancer Cell
Article

ROCK and JAK1 Signaling Cooperate to Control Actomyosin Contractility in Tumor Cells and Stroma

Victoria Sanz-Moreno,[1,12,9] Cedric Gaggioli,[2,3,12] Maggie Yeo,[1] Jean Albrengues,[2,3] Fredrik Wallberg,[4] Amaya Viros,[5] Steven Hooper,[6] Richard Mitter,[7] Chloé C. Féral,[8,3] Martin Cook,[10] James Larkin,[11] Richard Marais,[5] Guerrino Meneguzzi,[2,3] Erik Sahai,[6] and Chris J. Marshall[1,*]

[1]Oncogene Team, Institute of Cancer Research, Section of Cell and Molecular Biology, Cancer Research UK Tumour Cell Signalling Unit, 237 Fulham Road, London SW3 6JB, UK
[2]INSERM U634, IFR50, Faculté de Médecine
[3]Université de Nice Sophia-Antipolis, 28 Avenue de Valombrose
F-06107 Nice, France
[4]Institute of Cancer Research, Section of Cell and Molecular Biology, 237 Fulham Road, London SW3 6JB, UK
[5]Signal Transduction Team, Institute of Cancer Research, Section of Cell and Molecular Biology, Cancer Research UK Tumour Cell Signalling Unit, 237 Fulham Road, London SW3 6JB, UK
[6]Tumour Cell Biology Laboratory
[7]Bioinformatics and Biostatistics Service
Cancer Research UK London Research Institute, 44 Lincoln's Inn Fields, London WC2A 3PX, UK
[8]Equipe AVENIR, INSERM U634, IFR50, Faculté de Médecine, F-06107 Nice, France
[9]Randall Division of Cell and Molecular Biophysics, New Hunt's House, Guy's Campus, London SE1UL, UK
[10]Royal Surrey County Hospital, Guildford GU2 7XX, UK
[11]Skin Unit, Royal Marsden NHS Trust, Fulham Road, London SW36JJ, UK
[12]These authors contributed equally to this work
*Correspondence: chris.marshall@icr.ac.uk
DOI 10.1016/j.ccr.2011.06.018

SUMMARY

Proinflammatory cytokines are frequently observed in the tumor microenvironment, and chronic inflammation is involved in cancer initiation and progression. We show that cytokine signaling through the receptor subunit GP130-IL6ST and the kinase JAK1 generates actomyosin contractility through Rho-kinase dependent signaling. This pathway generates contractile force in stromal fibroblasts to remodel the extracellular matrix to create tracks for collective migration of squamous carcinoma cells and provides the high levels of actomyosin contractility required for migration of individual melanoma cells in the rounded, "amoeboid" mode. Thus, cytokine signaling can generate actomyosin contractility in both stroma and tumor cells. Strikingly, actomyosin contractility itself positively modulates activity of the transcription factor STAT3 downstream of JAK1, demonstrating positive feedback within the signaling network.

INTRODUCTION

Abnormal cell migration and invasion are key components of metastasis. Tumor cells can move either in a collective fashion or as individual cells (Friedl and Wolf, 2003a, 2003b, 2010; Wolf et al., 2003). The contractile force generated by actomyosin contractility has been shown to play a pivotal role in both collective and individual migration of tumor cells. Carcinoma-associated fibroblasts (CAFs) use contractile force and proteolytic activity to remodel the extracellular matrix to generate tracks for migration of cancer cells as collective strands led by a fibroblast (Gaggioli et al., 2007). Force-mediated matrix remodelling by CAFs depends on actomyosin contractility generated through Rho-Rho-kinase (ROCK) signaling (Gaggioli et al., 2007; Hooper et al., 2010). ROCK phosphorylates MYPT1, the targeting subunit of myosin phosphatase, resulting in decreased myosin phosphatase activity and thereby increased phosphorylation of the regulatory myosin light-chain 2 (MLC2) and activity of myosin II (Ito et al., 2004). High levels of Rho-ROCK signaling in tumor cells drive high levels of actomyosin contractility and are

Significance

Actomyosin contractility plays a key role in migration of tumor cells, both in the tumor cells themselves and in remodelling the extracellular matrix by tumor fibroblasts to permit cell migration. We show that cytokine signaling through GP130-IL6ST and JAK1 stimulates actomyosin contractility in tumor cells and in stroma. These results suggest that strategies to inhibit signaling through this axis may be effective to block different modes of tumor cell invasion.

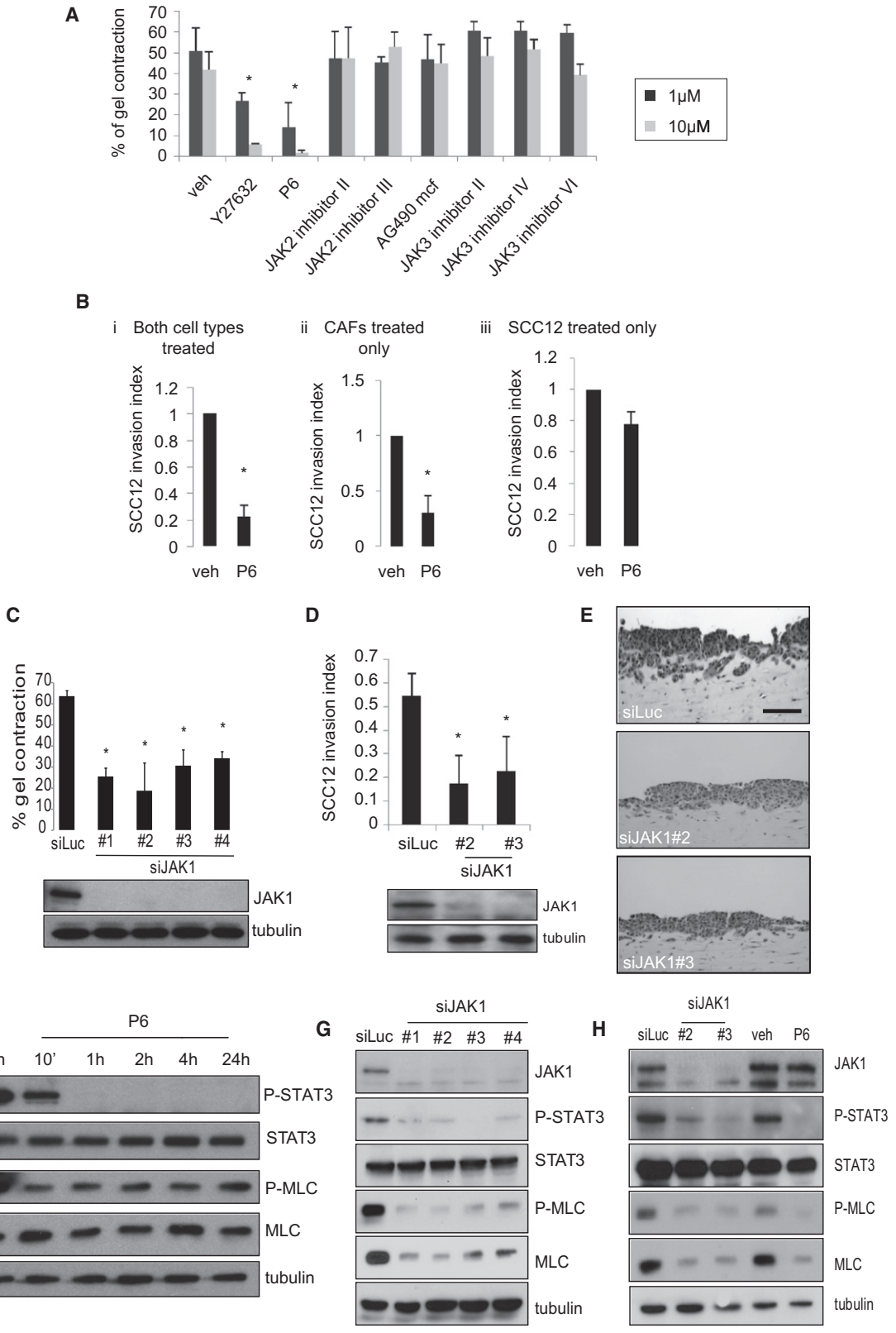

Figure 1. Janus Kinase Activity Is Required for CAF-Induced Matrix Remodelling and SCC12 Collective Invasion

(A) Matrix contraction by CAFs treated with: P6 (pan-JAK); JAK2 inhibitors II, III, and AG490 mcf; JAK3 inhibitors II, IV, and VI; and ROCK inhibitor Y27632. *$p < 0.01$.

associated with movement of individual cells in a rounded or "amoeboid" fashion; lower levels of contractility are associated with Rac-dependent elongated movement (Sahai and Marshall, 2003; Sanz-Moreno et al., 2008; Wilkinson et al., 2005; Wyckoff et al., 2006). The rounded, "amoeboid" form of movement occurs where the composition of the extracellular matrix allows the contractile force of the cell to deform the matrix (Friedl and Wolf, 2003a; Wyckoff et al., 2006). High actomyosin contractility may also provide cells with mechanical strength to resist shear forces following entry into the blood supply (Pinner and Sahai, 2008; Sanz-Moreno et al., 2008).

The signaling mechanisms generating contractile force in CAFs and tumor cells are not fully understood. It is unclear whether extracellular signals from growth factors or cytokines play a role and if they do what signaling pathways are engaged. In CAF-dependent ECM remodeling, it was recently shown that a kinase inhibitor, Pyridone 6 (P6) (Thompson et al., 2002), prevents CAF-dependent matrix remodeling (Hooper et al., 2010). P6 is an inhibitor of the JAK family kinases, JAK1, JAK2, JAK3, and TYK2, which are activated by cytokine-signaling pathways (Liu et al., 1997). This observation suggests that cytokine signaling may be involved in the generation of actomyosin contractility of CAFs. CAFs secrete a broad range of growth factors and cytokines (Kalluri and Zeisberg, 2006). Abnormal cytokine signaling is thought to play key roles in cancer because many studies have demonstrated a strong association between chronic inflammation and cancer (Aggarwal et al., 2009; Bromberg and Wang, 2009; Greten et al., 2004; Grivennikov and Karin, 2010). Cancer cells also produce cytokines that attract inflammatory cells, which also express a wide array of cytokines, proteases, and proinvasive extracellular matrix proteins (Coussens and Werb, 2002). Proinflammatory cytokines such as those of the interleukin-6 (IL-6) family (Erez et al., 2010; Kim et al., 2009; Melnikova and Bar-Eli, 2009; Rose-John et al., 2007) are frequently observed in the tumor microenvironment. IL-6 is a key driver in a mouse model of inflammation-associated colorectal cancer (Bollrath et al., 2009; Grivennikov et al., 2009) and provides an attractant for recruitment of circulating tumor cells (Kim et al., 2009). Cytokine signaling activates JAK family protein kinases resulting in tyrosine phosphorylation of substrates including the STAT (signal transducers and activators of transcription) family of transcription factors leading to the induction of gene expression (Pedranzini et al., 2004; Yu et al., 2009). STAT3 is constitutively activated in a variety of human malignancies, including prostate, lung, brain, breast, melanoma, and squamous cell carcinomas (Catlett-Falcone et al., 1999; Pedranzini et al., 2004), and is thought to be a key mediator of oncogenesis (Bromberg et al., 1999; Yu et al., 2009).

In the studies described here, we investigate whether cytokine signaling through JAK kinases is involved in generating actomyosin contractility in CAFs and melanoma cells.

RESULTS

JAK1 Regulates Actomyosin Contractility in CAFs and in Rounded Cell Movement

CAF-dependent matrix remodelling is essential for collective carcinoma cell invasion (Gaggioli et al., 2007). Screening for compounds that inhibit CAF-induced contraction of collagen lattices suggests a role for JAK signaling in matrix remodelling because the single JAK kinase inhibitor P6 tested blocked remodelling (Hooper et al., 2010). P6 inhibits multiple members of the JAK family (Pedranzini et al., 2006), so we used JAK isoform-specific inhibitors to probe which JAKs are involved; neither JAK2 nor JAK3-specific inhibitors recapitulated the effect of the pan-JAK inhibitor (P6) on matrix remodelling (Figure 1A), suggesting that JAKI is the family member involved.

To extend these results, we used an organotypic assay utilizing a squamous cell carcinoma cell line (SCC12) and CAFs (Gaggioli et al., 2007; Hooper et al., 2010). Figure 1B (panel i) shows that P6 dramatically blocked SCC invasion. In this assay it is possible to allow the CAFs to remodel the matrix before killing them and then adding tumor cells to the assay (Gaggioli et al., 2007). If CAFs were treated with P6 during matrix remodelling, SCC12 invasion was blocked (Figure 1Bii). However if untreated CAFs were allowed to remodel the matrix, killed, and then SCC12 cells added in the presence of P6, invasion was unaffected (Figure 1Biii). Thus, the effects of inhibiting JAK on collective invasion are on CAFs, not tumor cells. Treatment of CAFs with the JAK2-specific inhibitor SD1029 did not affect invasion (see Figure S1A available online). To confirm these results, we used RNA interference to abrogate expression of individual JAKs in CAFs. Figures 1C–1E and Figure S1B show that the RNAi-mediated knockdown of JAK1 dramatically reduced the capacity of CAFs to contract collagen lattices and induce SCC invasion. RNAi against JAK2 and TYK2 had no effect in these assays (Figure S1B; data not shown). Figures S1C–S1G show that treatment with P6 had no effect on viability, adhesion, MMP secretion, or the migration and invasion of CAFs into a 3D matrix. These results suggest that the effects of P6 on matrix remodelling are a consequence of inhibiting actomyosin contractility. Actomyosin contractility in CAFs, as in many other cell types, results from phosphorylation of MLC2 in myosin II downstream of the Rho kinases ROCK I and II (Gaggioli et al., 2007). To determine if JAKs regulate actomyosin contractility, we investigated phosphorylation of MLC2 following P6 treatment. Figure 1F shows that P6 reduces MLC2 phosphorylation

(B) Invasion of SCC12 cells after treatment with P6, (i) coculture of CAFs and SCC12 cells, (ii) acellular matrix from CAFs treated with P6 and overlaid with SCC12 cells, and (iii) acellular matrix from untreated CAFs, overlaid with SCC12 cells and treated with P6. *$p < 0.01$.
(C) Matrix contraction after siRNA depletion of JAK1 (n = 3, mean + SD; *$p < 0.01$). Bottom panel shows immunoblot for JAK1.
(D) Quantitation of organotypic invasion assays (n = 3, mean + SD; *$p < 0.01$). Bottom panel shows immunoblot for JAK1.
(E) Representative images of organotypic invasion assay. Scale bar, 100 μm.
(F) Immunoblot for P-MLC after treatment with P6.
(G) Immunoblot for P-STAT3 and P-MLC.
(H) Immunoblot for JAK1, P-STAT3, P-MLC, and MLC expression after transfection with siRNAs against JAK1 or P6 treatment for 96 hr.
See also Figure S1.

(P-MLC), whereas a specific JAK2 inhibitor had no effect (Figure S1H), suggesting that the JAK1 signals to MLC2 phosphorylation. Similarly, abrogating JAK1 expression with four different siRNAs reduced MLC2 phosphorylation (Figure 1G). Depletion of JAK1 by siRNA reduced total MLC2 levels; this appears to be a consequence of long-term abrogation of JAK1 signaling in CAFs because prolonged treatment with P6 also reduced total MLC2 levels (Figure 1H).

In movement of individual tumor cells rounded, ''amoeboid'' modes of movement are associated with high levels of actomyosin contractility (Wilkinson et al., 2005). A375M2 melanoma cells have high levels of MLC2 phosphorylation, a round, contractile morphology, and move in a rounded, ''amoeboid'' manner on top of or through deformable collagen matrices (Sanz-Moreno et al., 2008). Partial inhibition of actomyosin contractility results in elongated morphology and migration in a Rac-dependent protrusive manner (Sanz-Moreno et al., 2008). MLC2 phosphorylation in A375M2 cells was decreased following treatment with P6 (Figure 2A; Figure S2A) or depletion of JAK1 by siRNA (Figure 2B). The reduction in actomyosin contractility following P6 treatment or siRNA-mediated knockdown of JAK1 led to an elongated morphology (Figures 2C and 2D) similar to the effects of ROCK inhibition (Sanz-Moreno et al., 2008). Similar to CAFs, blocking JAK1 signaling in A375M2 melanoma cells had no effect on cell viability or adhesion (Figures S2B and S2C). Consistent with the effects on contractility, the proportion of cells with a round, contractile morphology was reduced, and elongated cells increased following treatment with P6 (Figure 2C) or by siRNA-mediated knockdown of JAK1 (Figures 2D and 2E). These elongated cells continued to move (Figure S2D). No increase in cell elongation was seen following targeting other members of the JAK family by siRNA (Figure S2E) or with a JAK2 inhibitor (data not shown). Thus, in both CAFs and melanoma cells, JAK1 signaling regulates actomyosin contractility by controlling the levels of phosphorylated-MLC2. On a rigid substrate where cells have an elongated shape, abrogation of JAK signaling led to increased membrane ruffles and cell flattening but no obvious effect on cell elongation (Figure S2F). JAK inhibition potentiated blockade of MLC2 phosphorylation by submaximal doses of ROCK inhibitor, consistent with JAK1 and ROCK operating in the same signaling pathway (data not shown)

GP130-IL6ST Regulates Actomyosin Contractility in CAFs and Tumor Cells

JAK1 can be activated by a variety of transmembrane receptors including cytokine receptors involved in inflammatory responses (O'Shea et al., 2002; Yamaoka et al., 2004). GP130-IL6ST is the common subunit for a number of cytokine receptors, and its expression has been correlated with matrix remodelling during neoangiogenesis (Salguero et al., 2009). We investigated the role of GP130-IL6ST in CAF-induced matrix contraction, SCC invasion, and rounded, ''amoeboid'' movement of tumor cells. Depletion of GP130-IL6ST in CAFs using siRNAs resulted in reduction of matrix contraction (Figure 3A), MLC2 phosphorylation (Figure S3A), and SCC12 invasion (Figures 3B and 3C). Thus, GP130-IL6ST signaling to JAK1 drives actomyosin contractility in CAFs and mediates matrix remodelling.

To investigate whether JAK1 signaling to MLC2 phosphorylation involves GP130-IL6ST in tumor cells, we depleted A375M2 cells of GP130-IL6ST by RNA interference. Depletion of GP130-IL6ST resulted in reduced MLC2 phosphorylation (Figures 3D and 3E). GP130-IL6ST depleted A375M2 cells invaded into a 3D collagen I matrix as elongated rather than round cells (Figures 3F and 3G) and had reduced invasive capacity (Figure S3B). Consistent with these changes in morphology of invaded cells, depletion of GP130-IL6ST by RNA interference resulted in reduction in the proportion of A375M2 cells on top of a collagen I matrix with a round, contractile morphology (Figures S3C and S3D and Movie S1). To extend these observations, we overexpressed GP130-IL6ST in SKMEL28 melanoma cells that have an elongated morphology and mode of invasion to see if overexpression would promote MLC2 phosphorylation and a round morphology. Overexpression of GP130-IL6ST resulted in an increased proportion of cells with a round, contractile morphology (Figures S3E and S3F). The increased proportion of cells with a round morphology resulting from overexpression of GP130 was blocked by P6 (Figure S3F). Interestingly, even in A375M2 cells where over 90% of cells have a round, contractile morphology, overexpression of GP130-IL6ST increased the proportion of round cells (data not shown). Overexpression of GP130-IL6ST led to increased MLC2 phosphorylation (Figures S3E and S3G) that was dependent on ROCK because it was blocked by the ROCK inhibitor H1152 (Figure S3G). Furthermore, overexpression of GP130-IL6ST led to a significant increase in invasion of SKMEL28 and A375M2 cells into a collagen I matrix (Figure S3H; data not shown).

To extend these results to migration of tumor cells in vivo, we used two-photon intravital imaging to examine the movement of cells in A375M2 xenografts. Imaging of two stable cell lines where GP130-IL6ST was depleted by expression of different shRNAs showed that tumor cell motility was significantly reduced compared to cells containing a control shRNA vector (Movie S2 and Movie S3). Figure 3H shows merged red, green, and blue images taken from three different time points 630 s apart in the time-lapse movies; spatial separation of colors indicates movement, whereas cells that do not migrate appear white (Pinner et al., 2009). Previous work has shown that in A375M2 tumors, cell movement at the periphery is predominantly rounded, ''amoeboid'' movement (Pinner and Sahai, 2008; Sanz-Moreno et al., 2008). Importantly, the reduction in motility of GP130-IL6ST depleted cells correlated with reduced levels of rounded, ''amoeboid'' movement (Figure 3I; Figure S3I). These data strongly support the argument that signaling through GP130-IL6ST and the JAK pathway drives rounded, ''amoeboid'' movement in culture and in vivo.

Cytokines of the IL-6 Family Regulate Actomyosin Contractility

The cytokine oncostatin M (OSM) signals through GP130-IL6ST and is a member of the IL-6 family. Because OSM signaling has been linked to adverse clinical outcome in squamous cell carcinoma (Ng et al., 2007), we investigated the role of OSM in matrix remodelling. Figures 4A and 4B show that stimulation of CAFs by OSM increased contraction of collagen lattices, whereas Figure 4C shows that OSM increased SCC12 cell invasion in the organotypic assay. These effects of OSM are mediated by JAK1 because they are eliminated by treatment with P6 or JAK1 siRNA, but not by JAK2 inhibitor SD1029 (Figures 4A–4C).

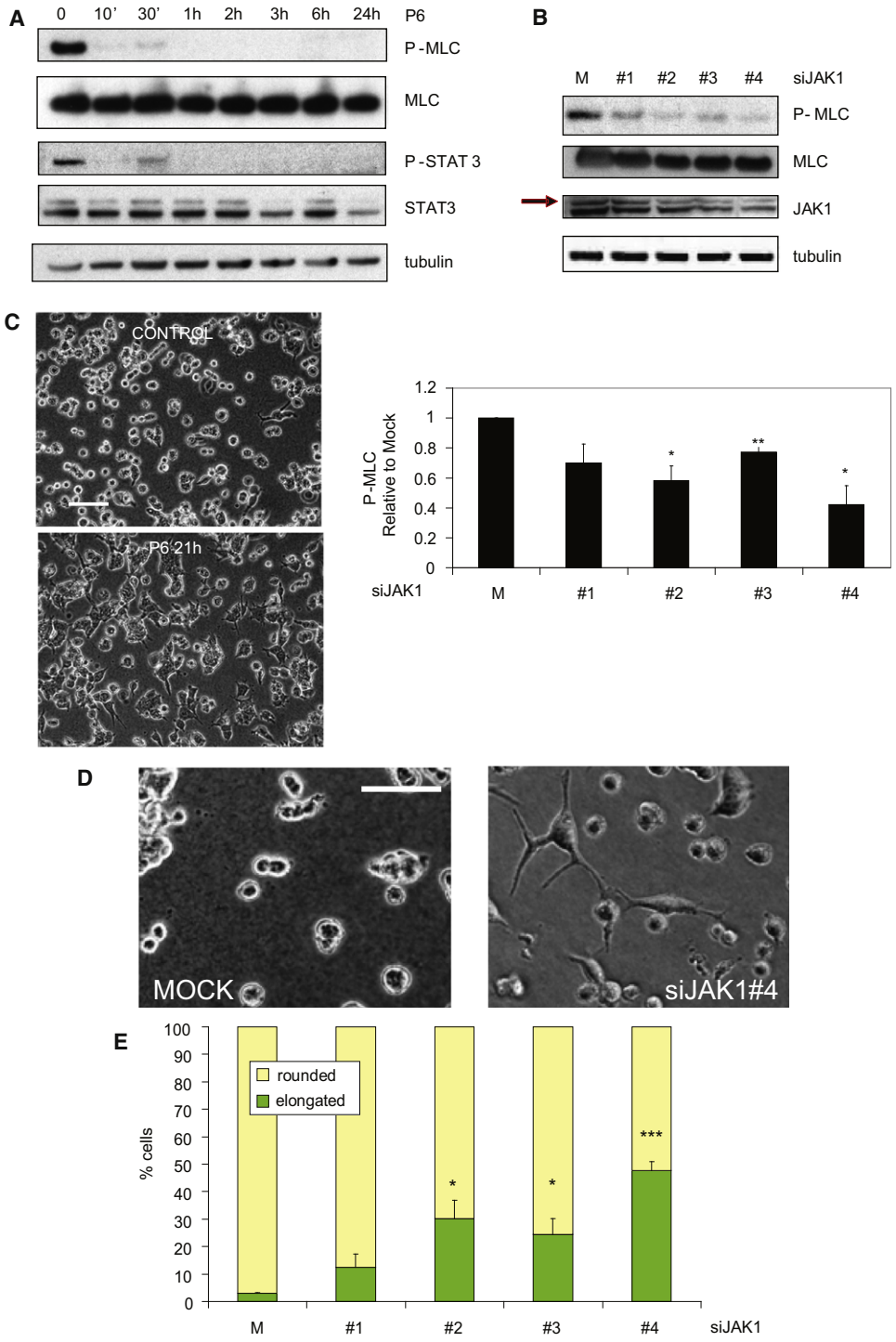

Figure 2. Jak Regulates Actomyosin Contractility in Amoeboid Cell Movement of Melanoma Cells

(A) Immunoblot of P-MLC in A375M2 cells on a thick layer of collagen and treated with P6.

(B) Upper panel shows immunoblot of P-MLC after depletion of JAK1, arrow shows position of JAK1, and lower panel quantification (n = 4, error bars are +SE; $^{**}p < 0.01$ and $^{*}p < 0.05$).

(C) Images of A375M2 cells plated on a thick layer of collagen for 24 hr and treated with P6. Scale bar represents 50 μm.

(D) Images of A375M2 cells after JAK1 depletion. Scale bar represents 50 μm.

(E) Percent (%) rounded and elongated cells after siRNA depletion of JAK1 (600 cells/experiment; n = 3, error bars are +SE). $^{*}p < 0.05$; $^{***}p < 0.005$.

See also Figure S2.

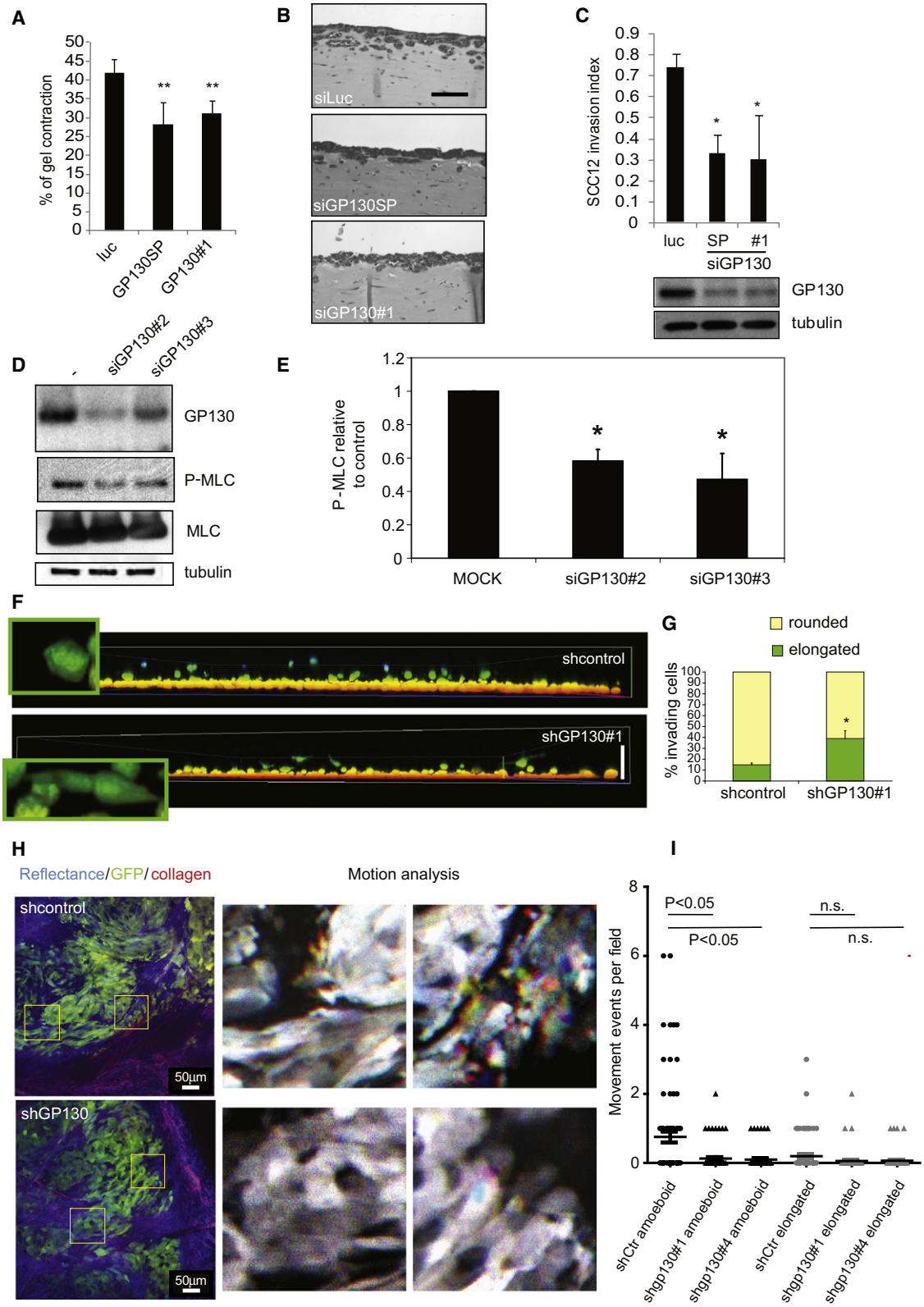

Figure 3. GP130-IL6ST Regulates CAF-Induced Matrix Remodelling, SCC12 Collective Invasion, and Actomyosin Contractility in Amoeboid Cell Movement

(A) Gel contraction by CAFs after siRNA depletion of GP130-IL6ST (n = 3, mean + SD; **p < 0.05).

(B) Representative images of organotypic invasion assays with CAFs depleted of GP130-IL6ST. Scale bar represents 100 µm.

Both basal and OSM stimulation of MLC2 phosphorylation are dependent on JAK1 signaling (Figures 4D and 4E) and ROCK (Figure 4D). Thus, OSM signaling through GP130-IL6ST, JAK1, and ROCK drives actomyosin contractility and matrix remodelling by CAFs for collective invasion of squamous cell carcinoma cells. Interestingly, P6 treatment also blocked basal gel contraction by CAFs (Figures 1A and 4A) and invasion by SCC12 cells (Figures 1B and 4C), indicating that under the conditions of these assays, in which complete media are used, the basal level of actomyosin contractility is mediated by JAK1 signaling (Figures 4D and 4E).

In melanoma, expression of IL-6 has been correlated with poor prognosis (Melnikova and Bar-Eli, 2009); therefore, we assessed if treatment of melanoma cells with IL-6 would affect cell morphology and mode of cell migration. We chose WM1361 cells where approximately 25% of cells invade into a 3D collagen I matrix with an elongated morphology and investigated whether IL-6 treatment would increase the proportion of cells invading in a rounded, ''amoeboid'' manner. IL-6 treatment led to an increase in the proportion of round cells and a 2-fold increase in invasion (Figures 4F and 4G). Treatment of three other melanoma cell lines, A375M2, WM1366, and SKMEL28, with IL-6 or leukemia inhibitory factor (LIF), which also signals through GP130-IL6ST (Gearing et al., 1992), resulted in increased invasion (Figures S4A and S4B). A375P and A375M2 cells plated on top of a collagen matrix and treated with IL-6 displayed an increase in the proportion of cells with a round, contractile morphology (Figures S4C and S4D). However, IL-6 stimulation, unlike OSM, had no effect on CAF-dependent gel contraction (Figure S4E) and STAT3 phosphorylation (Figure S4F), whereas it induced phosphorylation of STAT3 in SCC12 cells (Figure S4F). The absence of an IL-6 dependent response in CAFs compared to SCC12 cells may be explained by the low expression level of the IL-6 specific coreceptor GP80 in CAFs (Figure S4G).

Interplay between Actomyosin Contractility and JAK1-STAT3 Regulated Transcription

Key outputs of JAK signaling are tyrosine phosphorylation and activation of the STAT family of transcription factors (Bromberg et al., 1999; Yu et al., 2009). In the course of these experiments, we noted that treatment with ROCK inhibitors reduced phosphorylation of STAT3 both in CAFs (Figure 5A) and A375M2 cells (Figure 5B; Figure S5A). Therefore, we investigated whether activation of ROCK signaling leads to STAT3 phosphorylation. We used A375P cells expressing a ROCK-estrogen receptor fusion protein (ROCKER) to provide tamoxifen-inducible ROCK activity (Croft and Olson, 2006). Induction of ROCK activity resulted in STAT3 phosphorylation soon after tamoxifen treatment (Figure S5B) in a time frame similar to that for increased MLC2 phosphorylation. Induction of STAT3 phosphorylation by ROCK required kinase activity because a kinase-inactive version of ROCKER did not lead to inducible STAT3 phosphorylation (Figure S5B). STAT3 phosphorylation was inhibited by JAK inhibitor P6, showing that ROCK-induced STAT3 phosphorylation required JAK kinase activity (Figure S5C).

Accordingly, we assessed the role of STAT3 in CAF matrix remodeling and SCC12 cell invasion. In CAFs, STAT3 expression silencing using specific siRNA resulted in decreased matrix contraction (Figure 5C) and SCC12 cell invasion (Figures 5D and 5E). Figure 5F shows that, similar to JAK1 knockdown, STAT3 silencing in CAFs reduces the levels of phosphorylated and total MLC2 protein. The level of GP130-IL6ST protein expression was also decreased (Figure 5F), which suggests a possible positive regulatory loop via STAT3.

To investigate whether STAT factor signaling impacts on actomyosin contractility in A375M2 melanoma cells, we used as a readout of actomyosin contractility effects on the round, contractile cell morphology on top of a thick layer of collagen I. A375M2 cells were transfected with siRNAs targeting STAT1, STAT2, STAT3, STAT5A, or STAT5B; knockdown of STAT3 expression decreased the proportion of cells with round, contractile morphology (Figures 5G and 5H; Figure S5D). Depletion of STAT3 resulted in diminished levels of MLC2 phosphorylation (Figures 5I and 5J).

To examine if there are links among ROCK activity, actomyosin contractility, and STAT3-mediated transcriptional responses, we performed gene expression analysis. A375M2 cells were plated on top of a thick layer of collagen I and treated with ROCK inhibitors to reduce MLC2 phosphorylation or blebbistatin to directly inhibit Myosin II (Straight et al., 2003). To generate conditions of high actomyosin contractility, we plated cells on a thin layer of collagen I, where MLC2 phosphorylation is very high (Figure S6). In this gene expression analysis, we included A375P cells that have lower levels of MLC2 phosphorylation than A375M2 and have a predominantly elongated phenotype when plated on collagen (Sanz-Moreno et al., 2008). Genes upregulated in conditions of high contractility and downregulated in all treatments that decreased contractility are shown in Figure 6A. GeneGo Network Enrichment analysis (http://www.genego.com/metacore.php) showed that one of the main transcriptional networks in this data set is centered on the STAT family of transcription factors (Figure 6B) and includes genes such as GP130-IL6ST, the IL-6 receptor α subunit (IL6R), the cytokine LIF, and the LIF receptor α (LIFR). In confirmation of the gene expression data, in A375M2 cells treated with Y27632, H1152, blebbistatin, or in A375P cells, the protein

(C) Invasion index of SCC12 cells from assays as in (B) (n = 3, mean + SD; *p < 0.01). Bottom panel shows immunoblot for GP130-IL6ST.
(D) Immunoblots of P-MLC in A375M2 cells on thick collagen after siRNA depletion of GP130-IL6ST.
(E) Quantification of P-MLC levels (n = 3, error bars are +SE; *p < 0.05).
(F) Images of GFP-A375M2 cells stably transfected with shRNAs after 24 hr of invasion into collagen I. Scale bar represents 50 μm.
(G) Percent (%) rounded or elongated cells (n = 3, mean + SE; **p < 0.01).
(H) Multiphoton intravital microscopy of A375M2 subcutaneous tumors, and representative images of control (upper panels) and GP130-IL6ST shRNA (lower panels). Left-hand panels illustrate melanoma cells in green, collagen fibers in red, and reflective material in blue. Middle and right panels show at higher magnification motion analysis of areas indicated in yellow; red, green, and blue images from three time points 630 s apart are overlaid, and distinct areas of color indicate motile cells.
(I) Quantification of the number of motile cells in control and two different pools of GP130-IL6ST shRNA cells. ns, not significant.
See also Figure S3.

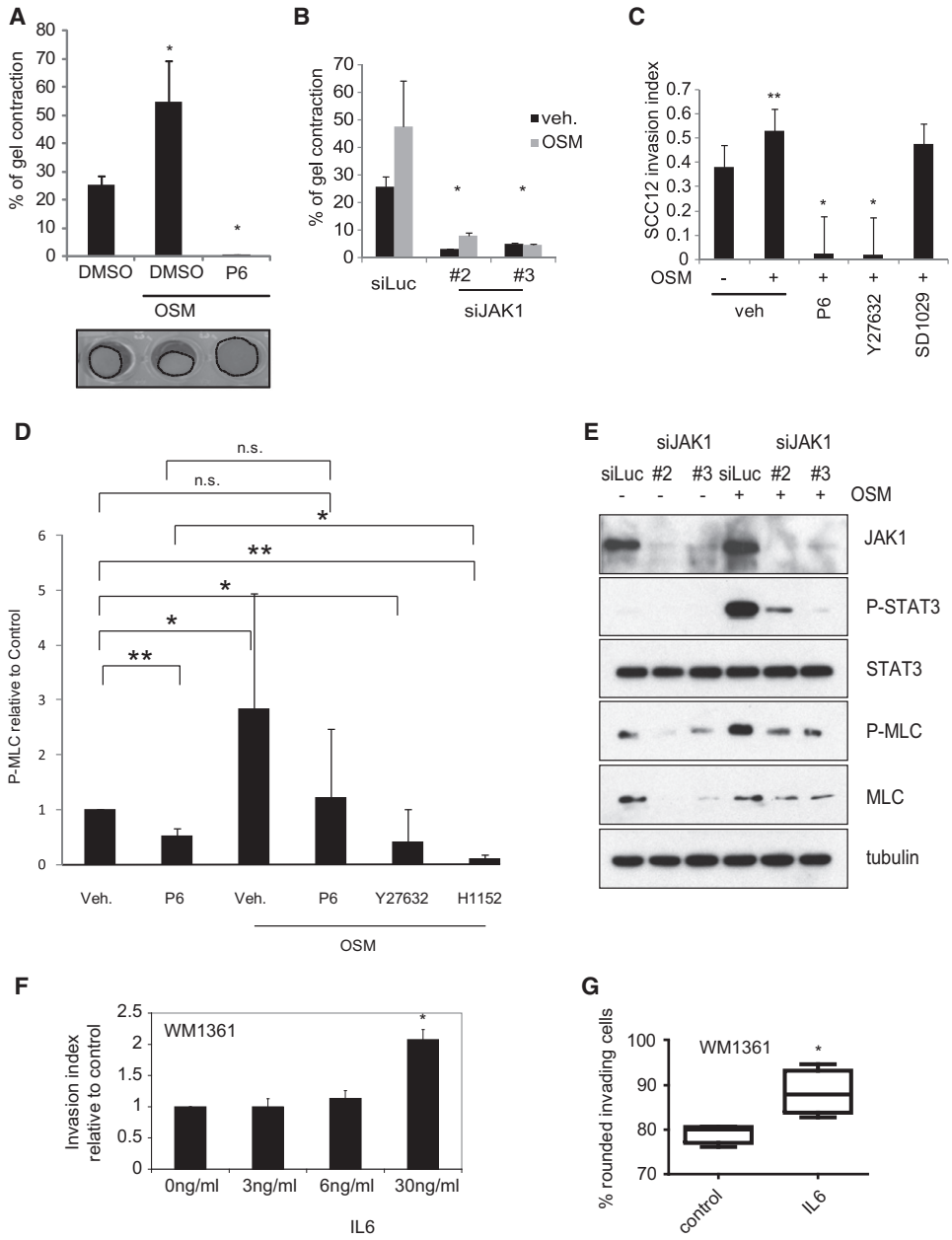

Figure 4. Cytokines of the IL-6 Family Regulate Actomyosin Contractility

(A) Matrix contraction by CAFs after exposure to 2 ng/ml OSM ± P6 (n = 3, mean + SD; *p < 0.01). Lower panel is representative image of contracted gels.

(B) Matrix contraction by CAFs after depletion of JAK1, ±2 ng/ml OSM (n = 3, mean + SD; *p < 0.01).

(C) SCC12 invasion after treatment with 2 ng/ml OSM ± P6 (n = 3, mean + SD; *p < 0.05 and **p < 0.01).

(D) Quantification of P-MLC levels in CAFs following 30 min treatment with 2 ng/ml OSM ± P6, Y27632, or H1152 treatment. Mean of five independent experiments +SD (*p < 0.05 and **p < 0.01). ns, not significant.

(E) Immunoblot of P-MLC from CAFs following 30 min treatment with 2 ng/ml OSM ± siRNAs against JAK1.

(F) Invasion index of WM1361 cells treated with IL-6 (n = 4; mean + SE; *p < 0.05).

(G) Box and whisker plot of morphology of GFP-WM1361 cells invading into collagen in the presence of 30 ng/ml IL-6 expressed as percent (%) rounded cells (n = 4; *p < 0.05).

See also Figure S4.

levels of secreted LIF and GP130-IL6ST were lower than in control cells (Figures 7A and 7B). Furthermore, ablation of JAK signaling also decreased expression of LIF and GP130-IL6ST (Figures S7A and S7B). To establish the role of some of these target genes, we used siRNA to silence expression of LIF, LIFR, and IL-6R; this resulted in a significant decrease in the levels of P-MLC (Figures 7C–7F). In accordance with these observations, the proportion of cells with a round, contractile

phenotype was also reduced (Figures 7G–7L). These results show that multiple components of the cytokine-signaling network like JAK1, GP130-IL6ST, and STAT3 are required to generate a highly contractile phenotype in A375M2 cells and that expression of some of these genes are regulated by ROCK and actomyosin contractility, providing evidence for positive feedback in the network.

It has been previously shown that GP130-IL6ST-JAK-STAT signaling establishes a positive feedback loop that impinges on the transcriptional regulation of components of the signaling network, and this is the basis for activation in tumors (Yu et al., 2009). STAT3 regulates its own expression (Snyder et al., 2008) and that of GP130-IL6ST (O'Brien and Manolagas, 1997). Consistent with these findings, JAK inhibitor treatment of A375M2 cells resulted in a significant decrease of GP130-IL6ST levels (Figure S7B) and STAT3 levels (Figure S7C). Likewise, activation of the GP130/IL6ST-JAK signaling through IL-6 stimulation resulted in an increase of STAT3 protein levels (Figure S7D) in A375M2 cells.

These results show that signaling through GP130-IL6ST, JAK, and STAT increases actomyosin contractility, and ROCK signaling to actomyosin contractility increases STAT3 phosphorylation and transcriptional responses. Thus, STAT3 signaling and actomyosin contractility are interdependent and cross-regulate each other (Figure S7E).

STAT3 Phosphorylation in Melanoma Correlates with Round Cell Morphology In Vivo

To examine if activation of the JAK1-STAT3 signaling pathway is correlated with a more contractile phenotype in melanomas in vivo, we first analyzed tumor xenografts of A375M2 and WM1361 melanoma cells in nude mice. Tumor sections were stained for phosphorylated STAT3 (P-STAT3) as a marker of activated JAK1-STAT3 signaling; cell morphology was assessed by dividing the shortest diameter of each cell by the longest one (ratio-b/ratio-a) to produce a score between 0 and 1, with perfectly round cells having a score of 1. Previous studies have shown that this is a valid approach for assessing the morphology of tumor cells in melanomas (Viros et al., 2008). Tumors from A375M2 cells had an average roundness score of 0.764 (SD = 0.17; $p < 0.0001$) compared to 0.52 (SD = 0.13; $p < 0.0001$) for WM1361 (Figure S8A). Figure S8B shows that A375M2 tumors compared to WM1361 tumors have a much higher percentage of tumor cells staining positive for P-STAT3 ($p = 0.000492$). Furthermore, the intensity of P-STAT3 staining was higher in A375M2 tumor sections than in WM1361 (Figures 8A and 8B). To further correlate staining with cell morphology, we assigned scores for P-STAT3 staining ranging from 0 (negative staining), 1–2 (moderate staining), and to 3 (intense staining). The cells with the highest degree of roundness in A375M2 tumors displayed the most intense staining (Figure 8A). Interestingly, even though WM1361 xenografts showed less overall staining for P-STAT3, we still observed a strong correlation between intensity of P-STAT3 staining and roundness (Figure 8B). We determined the role of GP130-IL6ST signaling in regulating morphology and degree of STAT3 phosphorylation in A375M2 cells in vivo. Analysis of the shape of cells in tumors derived from stable cell lines where GP130-IL6ST was depleted by expression of shRNA showed that they were more elongated than controls (Figure S8C). Furthermore, GP130-IL6ST depleted cells showed significantly less P-STAT3 staining than the controls, showing once more that STAT3 phosphorylation correlates with roundness (Figure S8C).

To extend these studies from subcutaneous xenografts to the clinical setting, we collected primary melanomas from 85 patients (Table S1). Because these studies involved a much larger series of samples, we estimated cell shape across whole tumor sections by obtaining a cell shape score in which we counted the percentage of cells in 4 categories ranging from 0 to 4 of increasing elongation (Experimental Procedures). This semiquantitative assessment has been shown to agree with the quantitative measurements of cell shape used in Figures 8A and 8B (Viros et al., 2008). Figures 8C and 8D show that the dermal invasive front of the majority of tumors consists of cells with a rounded morphology. Round cells predominated in the invasive front even when the cells in the body of the tumor had an elongated morphology (Figures 8C and 8D). These pathological findings closely mirror our imaging of A375M2 xenografts where the cells at the edge of the tumor abutting the interstitial matrix have a round morphology, and the cells in the body of the tumor are elongated (Figure 3H; Movie S2) (Sanz-Moreno et al., 2008). In no case did we find elongated cells in the invasive front when the tumor body consisted of primarily round cells. In accordance with our experimental findings that phosphorylation of STAT3 is associated with a round morphology and amoeboid-type movement, we found that there was a correlation between more intense P-STAT3 staining and round morphology in a set of 19 primary melanomas (Figure 8E). In many cases we could observe a gradient of P-STAT3 intensity toward the invasive front of primary tumors (Figure 8F). In tumors in which the body as well as the invasive front is composed of rounded cells, P-STAT3 was found throughout the tumor (Figure S8D).

Analysis of cell morphology from a subset of primary tumors for which we had metastases (n = 16) showed that metastases were often composed of more homogeneous round cell populations (Figure S8E). We examined cell morphology and P-STAT3 in metastases from three patients with melanoma (Table S2 shows clinical characteristics). In patient A the metastasis displayed a very elongated morphology with little staining for P-STAT3 (Figure S8F), whereas in patient B the cells had a predominantly round morphology and positive staining for P-STAT3 (Figure S8F and quantification in Figure S8G). We also examined two separate metastases from patient C that were surgically resected within a 3 year interval. Figure S8F shows that metastasis C1 showed cells with a predominantly elongated morphology and little staining for P-STAT3, whereas in metastasis C2 the cells were predominantly round and had higher staining for P-STAT3.

These observations show that in human melanoma samples as in cultured cells, activation of the JAK pathway is correlated with round cell morphology.

DISCUSSION

During tumor development, formation of abnormal microenvironment plays a crucial role in tumor cell proliferation, survival, and invasion (De Wever and Mareel, 2003). Both tumor and stromal cells contribute to formation of the microenvironment

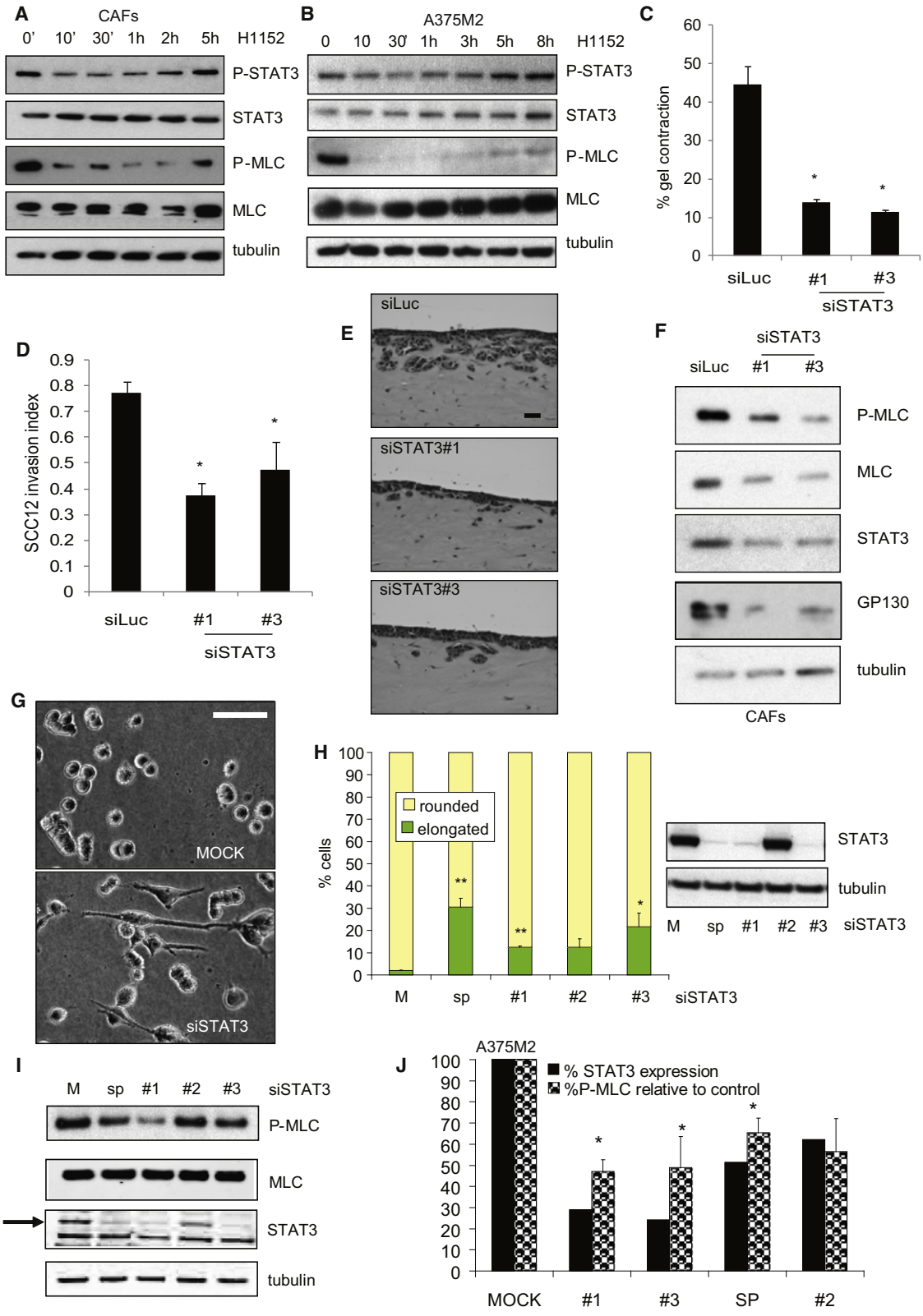

Figure 5. Rho Kinase Promotes STAT3 Phosphorylation

(A) Immunoblot of P-STAT3 and P-MLC in CAFs after treatment with H1152. (B) is as (A) for A375M2 cells after treatment with H1152. (C) Matrix contraction after 4 day depletion of STAT3 in CAFs (n = 3, mean + SD; *p < 0.01).

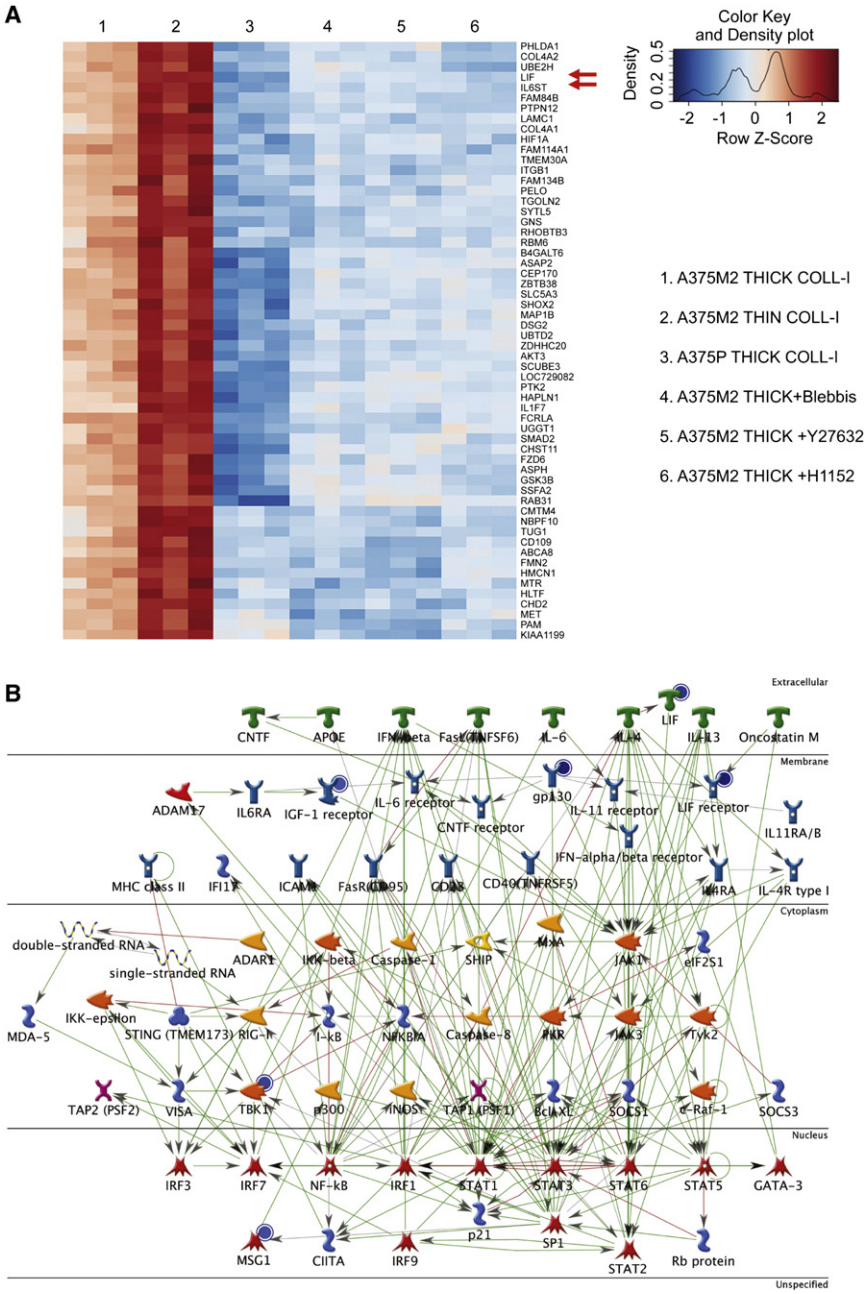

Figure 6. Rho Kinase and Actomyosin Contractility Promote STAT3-Dependent Transcriptional Responses

(A) Heat map of gene expression following inhibition of actomyosin contractility in A375M2 cells. Numbers at top indicate experimental condition. Genes upregulated in conditions of high contractility and downregulated in all treatments that decreased contractility are shown; blue indicates underexpression, red overexpression, and intensity of color indicates relative change. Red arrows point to GP130-IL6ST and LIF.

(B) Cytokine network following network enrichment analysis using MetaCore from GeneGo Inc. (http://www.genego.com/metacore.php). Downregulated genes are marked with blue circles comparing treatments and A375M2 cells on a thick layer of collagen I.

See also Figure S6.

(Coussens and Werb, 2002; Erez et al., 2010). Remodelling of the extracellular matrix involves metalloproteinases, integrins, and force generation by actomyosin contractility in stromal and tumor cells (Grinnell, 2003; Meshel et al., 2005) (Gaggioli et al., 2007) (Provenzano et al., 2006). Actomyosin contractility is also required to provide contractile force for tumor cell movement (Gaggioli et al., 2007) with high levels of actomyosin contractility driving rounded, "amoeboid" forms of individual cell movement (Sanz-Moreno et al., 2008). Strikingly, we find that the invasive fronts of melanomas mainly consist of rounded cells even though the body of the tumor may be made up of elongated cells (Figures 8C and 8D), arguing that melanoma cells at the invasive front are using the rounded, "amoeboid" form of cell movement.

Cytokine production is a key feature of the tumor microenvironment (Bromberg and Wang, 2009; Coussens and Werb, 2002; Erez et al., 2010); we show a role for cytokine signaling through GP130-IL6ST/JAK1 to regulate ROCK-dependent actomyosin contractility. This pathway drives matrix remodeling by CAFs and the rounded, "amoeboid" mode of migration of melanoma cells. Rounded melanoma cells stain strongly for P-STAT3, indicating activation of the JAK signaling pathway (Figure 8F). We show that multiple components of the cytokine network (Figure 6B) contribute to signaling to actomyosin contractility because silencing expression of GP130-IL6ST,

(D) SCC12 invasion assay after 7 day exposure of CAFs depleted for STAT3 (n = 3, mean + SD; *p < 0.01).
(E) Representative images of organotypic invasion assays with STAT3-depleted CAFs. Scale bar represents 50 μm.
(F) Immunoblot for P-MLC and GP130-IL6ST in STAT3-depleted CAFs.
(G) Images of A375M2 cells on thick collagen after siRNA depletion of STAT3. Scale bar represents 50 μm
(H) Percent (%) rounded and elongated cells in STAT3-depleted A375M2; 600 cells/experiment (n = 3, mean + SE). *p < 0.05; **p < 0.01.
(I) Immunoblot of P-MLC in STAT3-depleted A375M2.
(J) Quantification of P-MLC levels compared to STAT3 expression levels (n = 3, error bars are +SE; *p < 0.05) from (I).
See also Figure S5.

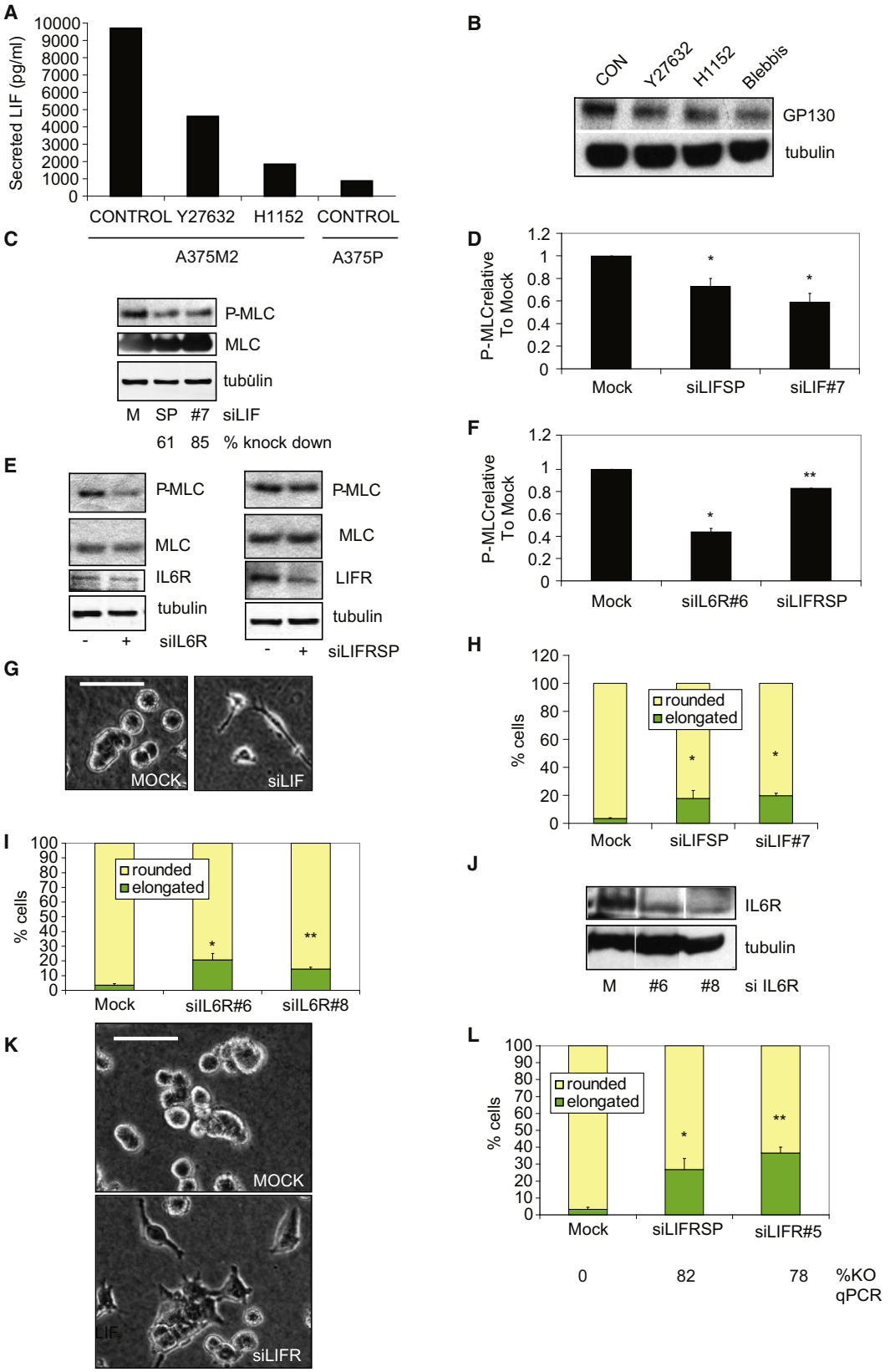
A
Secreted LIF (pg/ml)
10000
9000
8000
7000
6000
5000
4000
3000
2000
1000
0
CONTROL
Y27632
H1152
CONTROL
A375M2
A375P
B
CON
Y27632
H1152
Blebbis
GP130
tubulin
C
P-MLC
MLC
tubulin
M
SP
#7
siLIF
61
85
% knock down
D
P-MLCrelative To Mock
1.2
1
0.8
0.6
0.4
0.2
0
Mock
siLIFSP
siLIF#7
E
P-MLC
MLC
IL6R
tubulin
-
+
siIL6R
P-MLC
MLC
LIFR
tubulin
-
+
siLIFRSP
F
P-MLCrelative To Mock
1.2
1
0.8
0.6
0.4
0.2
0
Mock
siIL6R#6
siLIFRSP
G
MOCK
siLIF
H
% cells
120
100
80
60
40
20
0
rounded
elongated
Mock
siLIFSP
siLIF#7
I
% cells
100
90
80
70
60
50
40
30
20
10
0
rounded
elongated
Mock
siIL6R#6
siIL6R#8
J
IL6R
tubulin
M
#6
#8
si IL6R
K
MOCK
LIF
siLIFR
L
% cells
100
90
80
70
60
50
40
30
20
10
0
rounded
elongated
Mock
siLIFRSP
siLIFR#5
0
82
78
%KO qPCR

JAK1, the cytokine LIF, its specific receptor LIFR, and the specific IL-6 receptor IL-6R (GP80) all reduce actomyosin contractility in melanoma cells (Figure 7). In CAFs we show that the cytokine OSM signaling through GP130-IL6ST stimulates actomyosin contractility. Interestingly, OSM is known to induce lung and liver fibrosis (Mozaffarian et al., 2008), and epithelial-mesenchymal transition to a myofibroblastic phenotype (Nightingale et al., 2004), predisposing factors to cancer (Radisky et al., 2007). Unlike melanoma cells where the GP130-IL6ST/JAK1-ROCK signaling is required for tumor cell movement, in collective invasion of squamous cell carcinoma cells, this pathway is not required in the tumor cells but is required in CAFs to remodel the matrix.

A link between JAK signaling and actomyosin contractility has recently been demonstrated in vascular smooth muscle cells where angiotensin II, acting through the G protein-coupled AT1 receptor, activates JAK2 that phosphorylates a Rho guanine nucleotide exchange factor, ARHGEF1, to activate RhoA to the GTP-bound state. This leads to activation of ROCK and consequent phosphorylation of MLC2 (Guilluy et al., 2010). In CAFs and melanoma cells, signaling through JAK1 may involve some of the same elements as in vascular smooth muscle cells because we have found that basal RhoA activity in CAFs is sensitive to inhibition of JAK (Figure S7F), and OSM stimulates RhoA activation in a JAK-dependent manner (Figure S7G). Importantly, we show that in melanomas in vivo, the round, contractile morphology associated with high actomyosin contractility is associated with P-STAT3 (Figure 8; Figure S8). In tumor cells we show that transcriptional responses mediated by STAT3 are involved in the generation of actomyosin contractility. A key role of the STAT3 transcriptional response is to regulate the expression of GP130-IL6ST, the common subunit of cytokine receptors required for JAK activation. Overlaid on JAK-STAT3 signaling is an input from ROCK that regulates the phosphorylation status of STAT3. Previous studies have shown that Rho signaling positively influences STAT3 phosphorylation (Aznar et al., 2001), but it was not known which Rho-dependent signaling pathway is involved. Thus, JAK signaling activates ROCK, then ROCK and actomyosin contractility enhance STAT3 phosphorylation. Therefore, there is positive feedback from STAT3 to GP130-IL6ST expression and JAK activity, resulting in ROCK activation and enhanced STAT3 phosphorylation (see Figure S7E). Such an organization may provide the basis for sustained signaling responses required for the process of invasion that takes place over a prolonged time scale.

STAT3 activation has been reported to be involved in tumor invasion (Xiong et al., 2008; Yakata et al., 2007; Zhao et al., 2008) and regulates the expression of matrix metalloproteinases MMP-1, MMP-2, and MMP9 (Itoh et al., 2006; Song et al., 2008; Xie et al., 2004) and MUC1 (Gaemers et al., 2001), all of which have roles in tumor invasion. It is striking that we find that STAT3 phosphorylation in melanoma cells is associated with the round morphology consequent on high levels of actomyosin contractility that is linked to a more aggressive phenotype (Viros et al., 2008).

High levels of cytokines are found in melanomas, squamous cell carcinomas, and other tumors (Melnikova and Bar-Eli, 2009; van Kempen et al., 2003). In melanoma, IL-6 has been shown to be upregulated in disease progression (Moretti et al., 1999) and may be produced by tumor cells or within the tumor microenvironment (Melnikova and Bar-Eli, 2009). As well as in tumor cells, we find P-STAT3 in tumor-associated cells such as inflammatory cells, fibroblasts, and endothelial cells (Chen et al., 2008) in human melanomas (Figure S8H).

Our studies reveal roles for cytokine signaling in mediating cancer cell dissemination both in force-mediated matrix remodelling by CAFs and in amoeboid motility of tumor cells. These results suggest that blocking cytokine-signaling pathways may impinge on tumor cell invasion as well as proliferation and survival. Therapeutic agents such as blocking antibodies against cytokines (Rose-John et al., 2007) or small molecule inhibitors of JAK kinase (Pedranzini et al., 2006) or STAT activity (Yue and Turkson, 2009) may be useful agents to block invasion and metastasis.

EXPERIMENTAL PROCEDURES

Cell Culture

CAFs were cultured from a resection of an oral SCC in 10% FCS and DMEM (Gaggioli et al., 2007). SCC12 cells were cultured in FAD media. Melanoma cells were maintained in DMEM or RPMI containing 10% fetal calf serum.

Cell Culture on Thick Layers of Collagen and Time-Lapse Phase-Contrast Microscopy

Fibrillar bovine dermal collagen was prepared at 1.7 mg/ml in DMEM according to the manufacturer's protocol (Cohesion, Palo Alto, CA): 300 μl/well in 24-well plates, 700 μl/well in 12-well plates. Melanoma cells were seeded on top of collagen in medium containing 10% serum, allowed to adhere for 24 hr, and medium was changed to 1% serum for 16 hr. When calculating P-MLC levels relative to mock or control, tubulin levels were used for normalization.

Figure 7. A Network Centered on STAT3 Regulates Actomyosin Contractility

(A) Secreted LIF in A375M2 cells treated with ROCK inhibitors.
(B) Immunoblot for GP130-IL6ST after treatment of A375M2 cells with ROCK inhibitors or blebbistatin.
(C) Immunoblot for P-MLC after LIF depletion by siRNA.
(D) Quantification of P-MLC levels (n = 4, mean + SE).
(E) Immunoblot for P-MLC after IL-6R or LIFR depletion by siRNA.
(F) Quantification of P-MLC levels (n = 4, mean + SE).
(G) Images of A375M2 depleted of LIF by siRNA. Scale bar represents 50 μm.
(H) Percent (%) rounded and elongated A375M2 cells after depletion of LIF by siRNA.
(I) Percent (%) rounded and elongated A375M2 cells after depletion of IL-6R by siRNA (600 cells/experiment, n = 3, mean + SE).
(J) Immunoblot for IL-6R.
(K) Images of A375M2 depleted of LIFR by siRNA. Scale bar represents 50 μm.
(L) Percent (%) rounded and elongated A375M2 cells after depletion of LIFR by siRNAs. LIFR KO is shown by qPCR analysis.
In (H), (I), and (L), 600 cells/experiment (n = 3, mean + SE). Student's t test, $^{**}p < 0.01$ and $^{*}p < 0.05$ in (D), (F), (H), (I), and (L). See also Figure S7.

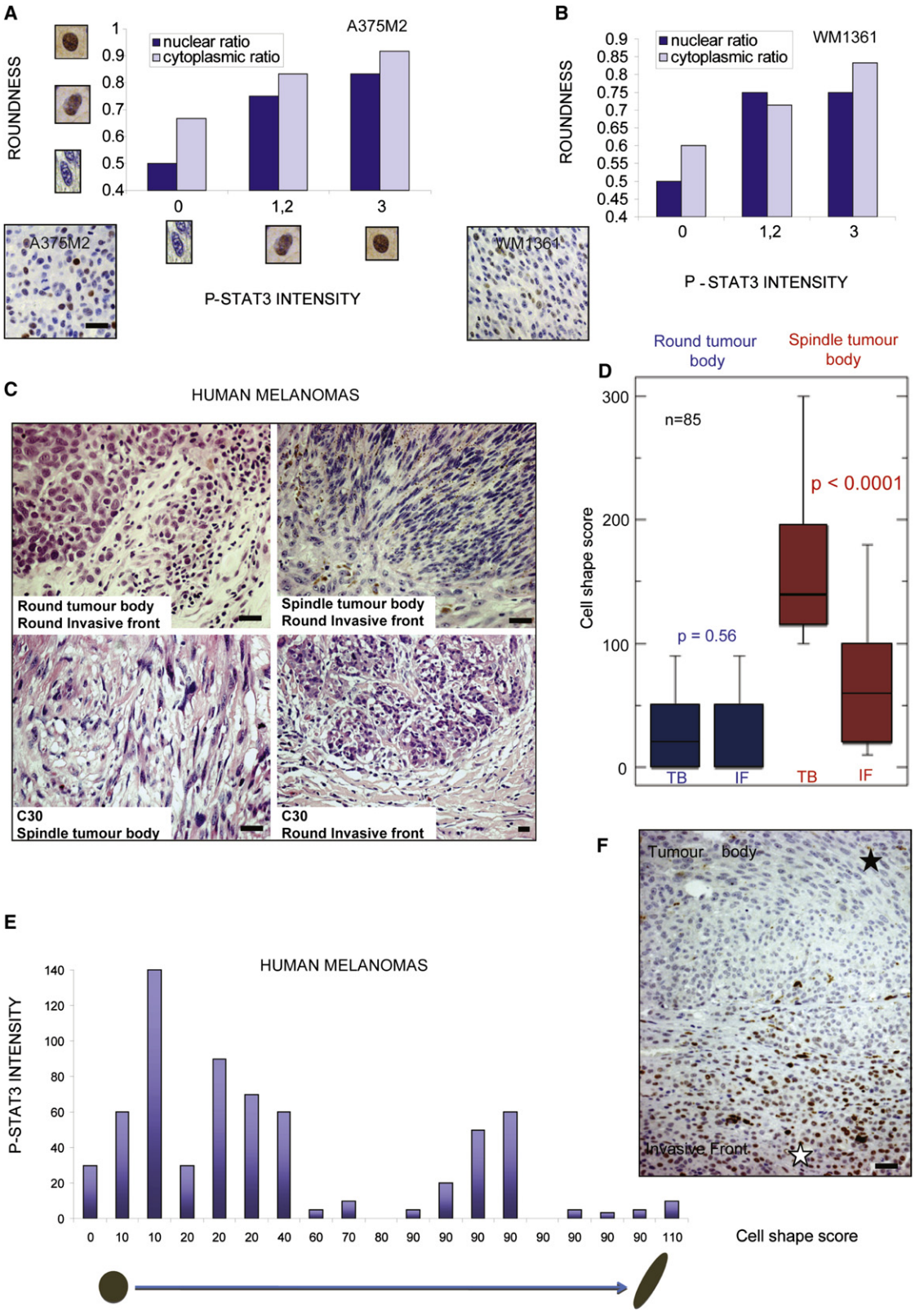

Figure 8. STAT3 Phosphorylation Correlates with a Contractile Phenotype In Vivo

(A and B) (A) Histogram of roundness versus intensity of P-STAT3 staining in A375M2 subcutaneous tumors. (B) is as (A) for WM1361 tumors (n = 100 cells/tumor; Kruskal-Wallis, $p < 0.0001$). P-STAT3 staining in sections from A375M2 or WM1361 tumors is shown.

Cytokine Measurements

LIF levels were measured using BD CBA (Cytometric Bead Array) Functional Bead system.

Tumor Imaging

Nude mice were injected subcutaneously, and when tumors were 3–7 mm in diameter, mice were anesthetized and imaged as described (Wyckoff et al., 2006). All animal experiments were carried out under license from the Home Office, UK.

Microarray

RNA was extracted from cells seeded on top of collagen using TRIzol (Invitrogen, Carlsbad, CA) followed by QIAGEN RNeasy Midi Kit. cRNA was prepared according to the GeneChip Expression Analysis Technical Manual (Affymetrix), hybridized onto HU133A chips (Affymetrix), and scanned by a GeneArray 2500 Scanner (Affymetrix). Network and enrichment analysis of the gene lists was performed using MetaCore from GeneGo Inc. (http://www.genego.com/metacore.php).

Patient Samples

Hematoxylin and eosin-stained slides assessed belong to the archives of the Royal Surrey County Hospital UK and Royal Marsden Hospital Foundation Trust. Slides were coded and uncoupled from personal identifiers. Staining for P-STAT3 was performed on surplus paraffin-embedded archival material. All procedures using human tissues were approved by the Ethics Committees of the Institute of Cancer Research and the Royal Marsden Hospital Foundation Trust and Royal Surrey County Hospital UK in accordance with the Human Tissue Act 2004.

Statistical Analyses

Student's t test was performed for quantifications of P-MLC, percent (%) elongated or rounded-type cells, and invasive index; ** indicates $p < 0.01$, and * indicates $p < 0.05$. Error bars are plus standard error (+SE). For the in vivo scatter plot in Figure 3I, the Mann-Whitney U test was used.

ACCESSION NUMBERS

Gene microarray data are deposited at the NCBI Gene Expression Omnibus (http://www.ncbi.nlm.nih.gov/geo) with accession numbers GSM586484–GSM586501.

SUPPLEMENTAL INFORMATION

Supplemental Information includes eight figures, two tables, three movies, and Supplemental Experimental Procedures and can be found with this article online at doi:10.1016/j.ccr.2011.06.018.

ACKNOWLEDGMENTS

This work was supported by Cancer Research UK, the EU, and the French Society of Dermatological Research (SRD). C.J.M. is a Cancer Research UK Gibb fellow, V.S.-M. is a CRUK Career Development Fellow, and C.G. is recipient of an INSERM CDD young researcher award. We acknowledge NHS funding to the NIHR Biomedical Research Centre. We thank Etienne Boulter, Amel Mettouchi, Mike Olson, and Eduardo Artz for reagents. We thank Hugh Paterson for advice on microscopy, Kay Savage and Eric Ward for histological analysis, Afshan McCarthy for assistance with mouse experiments, and Catherine Pons for technical assistance.

Received: August 7, 2010
Revised: March 11, 2011
Accepted: June 23, 2011
Published: August 15, 2011

REFERENCES

Aggarwal, B.B., Vijayalekshmi, R.V., and Sung, B. (2009). Targeting inflammatory pathways for prevention and therapy of cancer: short-term friend, long-term foe. Clin. Cancer Res. *15*, 425–430.

Aznar, S., Valerón, P.F., del Rincon, S.V., Pérez, L.F., Perona, R., and Lacal, J.C. (2001). Simultaneous tyrosine and serine phosphorylation of STAT3 transcription factor is involved in Rho A GTPase oncogenic transformation. Mol. Biol. Cell *12*, 3282–3294.

Bollrath, J., Phesse, T.J., von Burstin, V.A., Putoczki, T., Bennecke, M., Bateman, T., Nebelsiek, T., Lundgren-May, T., Canli, O., Schwitalla, S., et al. (2009). gp130-mediated Stat3 activation in enterocytes regulates cell survival and cell-cycle progression during colitis-associated tumorigenesis. Cancer Cell *15*, 91–102.

Bromberg, J., and Wang, T.C. (2009). Inflammation and cancer: IL-6 and STAT3 complete the link. Cancer Cell *15*, 79–80.

Bromberg, J.F., Wrzeszczynska, M.H., Devgan, G., Zhao, Y., Pestell, R.G., Albanese, C., and Darnell, J.E., Jr. (1999). Stat3 as an oncogene. Cell *98*, 295–303.

Catlett-Falcone, R., Landowski, T.H., Oshiro, M.M., Turkson, J., Levitzki, A., Savino, R., Ciliberto, G., Moscinski, L., Fernández-Luna, J.L., Nuñez, G., et al. (1999). Constitutive activation of Stat3 signaling confers resistance to apoptosis in human U266 myeloma cells. Immunity *10*, 105–115.

Chen, S.H., Murphy, D.A., Lassoued, W., Thurston, G., Feldman, M.D., and Lee, W.M. (2008). Activated STAT3 is a mediator and biomarker of VEGF endothelial activation. Cancer Biol. Ther. *7*, 1994–2003.

Coussens, L.M., and Werb, Z. (2002). Inflammation and cancer. Nature *420*, 860–867.

Croft, D.R., and Olson, M.F. (2006). Conditional regulation of a ROCK-estrogen receptor fusion protein. Methods Enzymol. *406*, 541–553.

De Wever, O., and Mareel, M. (2003). Role of tissue stroma in cancer cell invasion. J. Pathol. *200*, 429–447.

Erez, N., Truitt, M., Olson, P., Arron, S.T., and Hanahan, D. (2010). Cancer-associated fibroblasts are activated in incipient neoplasia to orchestrate tumor-promoting inflammation in an NF-kappaB-dependent manner. Cancer Cell *17*, 135–147, Erratum: (2010). Cancer Cell *17*, 523.

Friedl, P., and Wolf, K. (2003a). Proteolytic and non-proteolytic migration of tumour cells and leucocytes. Biochem. Soc. Symp. *70*, 277–285.

Friedl, P., and Wolf, K. (2003b). Tumour-cell invasion and migration: diversity and escape mechanisms. Nat. Rev. Cancer *3*, 362–374.

Friedl, P., and Wolf, K. (2010). Plasticity of cell migration: a multiscale tuning model. J. Cell Biol. *188*, 11–19.

Gaemers, I.C., Vos, H.L., Volders, H.H., van der Valk, S.W., and Hilkens, J. (2001). A stat-responsive element in the promoter of the episialin/MUC1 gene is involved in its overexpression in carcinoma cells. J. Biol. Chem. *276*, 6191–6199.

(C) H&E of patient tumors. Left upper panels show round cell tumor body with an invasive front of round cells; right illustrate spindle cell tumor body with an invasive front of round cells. Lower panels show another tumor with spindle-shaped cells in tumor body and round cells in the invasive front. Scale bars represent 30 μm.
(D) Quantification of cell shape score from 85 primary invasive malignant melanomas: cell shape score = ((percentage of cells [%] shape 0 × 0) + (% shape 1 × 1) + (% shape 2 × 2) + (% shape 3 × 3)), with values ranging from 0 (all cells round) to 300 (all cells spindle).
(E) Intensity of P-STAT3 and cell shape in a subset of 19 samples (Wilcoxon signed-rank test, $p = 0.0293$).
(F) Image of P-STAT3 staining in a section from a patient with melanoma. Black star represents elongated and spindle cells in the tumor body with no P-STAT3 staining. White star indicates round cells in the invasive front staining for P-STAT3. Scale bar represents 100 μm.
See also Figure S8.

Gaggioli, C., Hooper, S., Hidalgo-Carcedo, C., Grosse, R., Marshall, J.F., Harrington, K., and Sahai, E. (2007). Fibroblast-led collective invasion of carcinoma cells with differing roles for RhoGTPases in leading and following cells. Nat. Cell Biol. *9*, 1392–1400.

Gearing, D.P., Comeau, M.R., Friend, D.J., Gimpel, S.D., Thut, C.J., McGourty, J., Brasher, K.K., King, J.A., Gillis, S., Mosley, B., et al. (1992). The IL-6 signal transducer, gp130: an oncostatin M receptor and affinity converter for the LIF receptor. Science *255*, 1434–1437.

Greten, F.R., Eckmann, L., Greten, T.F., Park, J.M., Li, Z.W., Egan, L.J., Kagnoff, M.F., and Karin, M. (2004). IKKbeta links inflammation and tumorigenesis in a mouse model of colitis-associated cancer. Cell *118*, 285–296.

Grinnell, F. (2003). Fibroblast biology in three-dimensional collagen matrices. Trends Cell Biol. *13*, 264–269.

Grivennikov, S.I., and Karin, M. (2010). Inflammation and oncogenesis: a vicious connection. Curr. Opin. Genet. Dev. *20*, 65–71.

Grivennikov, S., Karin, E., Terzic, J., Mucida, D., Yu, G.Y., Vallabhapurapu, S., Scheller, J., Rose-John, S., Cheroutre, H., Eckmann, L., and Karin, M. (2009). IL-6 and Stat3 are required for survival of intestinal epithelial cells and development of colitis-associated cancer. Cancer Cell *15*, 103–113.

Guilluy, C., Brégeon, J., Toumaniantz, G., Rolli-Derkinderen, M., Retailleau, K., Loufrani, L., Henrion, D., Scalbert, E., Bril, A., Torres, R.M., et al. (2010). The Rho exchange factor Arhgef1 mediates the effects of angiotensin II on vascular tone and blood pressure. Nat. Med. *16*, 183–190.

Hooper, S., Gaggioli, C., and Sahai, E. (2010). A chemical biology screen reveals a role for Rab21-mediated control of actomyosin contractility in fibroblast-driven cancer invasion. Br. J. Cancer *102*, 392–402.

Ito, M., Nakano, T., Erdodi, F., and Hartshorne, D.J. (2004). Myosin phosphatase: structure, regulation and function. Mol. Cell. Biochem. *259*, 197–209.

Itoh, M., Murata, T., Suzuki, T., Shindoh, M., Nakajima, K., Imai, K., and Yoshida, K. (2006). Requirement of STAT3 activation for maximal collagenase-1 (MMP-1) induction by epidermal growth factor and malignant characteristics in T24 bladder cancer cells. Oncogene *25*, 1195–1204.

Kalluri, R., and Zeisberg, M. (2006). Fibroblasts in cancer. Nat. Rev. Cancer *6*, 392–401.

Kim, M.Y., Oskarsson, T., Acharyya, S., Nguyen, D.X., Zhang, X.H., Norton, L., and Massagué, J. (2009). Tumor self-seeding by circulating cancer cells. Cell *139*, 1315–1326.

Liu, K.D., Gaffen, S.L., Goldsmith, M.A., and Greene, W.C. (1997). Janus kinases in interleukin-2-mediated signaling: JAK1 and JAK3 are differentially regulated by tyrosine phosphorylation. Curr. Biol. *7*, 817–826.

Melnikova, V.O., and Bar-Eli, M. (2009). Inflammation and melanoma metastasis. Pigment Cell Melanoma Res. *22*, 257–267.

Meshel, A.S., Wei, Q., Adelstein, R.S., and Sheetz, M.P. (2005). Basic mechanism of three-dimensional collagen fibre transport by fibroblasts. Nat. Cell Biol. *7*, 157–164.

Moretti, S., Pinzi, C., Spallanzani, A., Berti, E., Chiarugi, A., Mazzoli, S., Fabiani, M., Vallecchi, C., and Herlyn, M. (1999). Immunohistochemical evidence of cytokine networks during progression of human melanocytic lesions. Int. J. Cancer *84*, 160–168.

Mozaffarian, A., Brewer, A.W., Trueblood, E.S., Luzina, I.G., Todd, N.W., Atamas, S.P., and Arnett, H.A. (2008). Mechanisms of oncostatin M-induced pulmonary inflammation and fibrosis. J. Immunol. *181*, 7243–7253.

Ng, G., Winder, D., Muralidhar, B., Gooding, E., Roberts, I., Pett, M., Mukherjee, G., Huang, J., and Coleman, N. (2007). Gain and overexpression of the oncostatin M receptor occur frequently in cervical squamous cell carcinoma and are associated with adverse clinical outcome. J. Pathol. *212*, 325–334.

Nightingale, J., Patel, S., Suzuki, N., Buxton, R., Takagi, K.I., Suzuki, J., Sumi, Y., Imaizumi, A., Mason, R.M., and Zhang, Z. (2004). Oncostatin M, a cytokine released by activated mononuclear cells, induces epithelial cell-myofibroblast transdifferentiation via Jak/Stat pathway activation. J. Am. Soc. Nephrol. *15*, 21–32.

O'Brien, C.A., and Manolagas, S.C. (1997). Isolation and characterization of the human gp130 promoter. Regulation by STATS. J. Biol. Chem. *272*, 15003–15010.

O'Shea, J.J., Gadina, M., and Schreiber, R.D. (2002). Cytokine signaling in 2002: new surprises in the Jak/Stat pathway. Cell Suppl. *109*, S121–S131.

Pedranzini, L., Leitch, A., and Bromberg, J. (2004). Stat3 is required for the development of skin cancer. J. Clin. Invest. *114*, 619–622.

Pedranzini, L., Dechow, T., Berishaj, M., Comenzo, R., Zhou, P., Azare, J., Bornmann, W., and Bromberg, J. (2006). Pyridone 6, a pan-Janus-activated kinase inhibitor, induces growth inhibition of multiple myeloma cells. Cancer Res. *66*, 9714–9721.

Pinner, S., and Sahai, E. (2008). Imaging amoeboid cancer cell motility in vivo. J. Microsc. *231*, 441–445.

Pinner, S., Jordan, P., Sharrock, K., Bazley, L., Collinson, L., Marais, R., Bonvin, E., Goding, C., and Sahai, E. (2009). Intravital imaging reveals transient changes in pigment production and Brn2 expression during metastatic melanoma dissemination. Cancer Res. *69*, 7969–7977.

Provenzano, P.P., Eliceiri, K.W., Campbell, J.M., Inman, D.R., White, J.G., and Keely, P.J. (2006). Collagen reorganization at the tumor-stromal interface facilitates local invasion. BMC Med. *4*, 38.

Radisky, D.C., Kenny, P.A., and Bissell, M.J. (2007). Fibrosis and cancer: do myofibroblasts come also from epithelial cells via EMT? J. Cell. Biochem. *101*, 830–839.

Rose-John, S., Waetzig, G.H., Scheller, J., Grötzinger, J., and Seegert, D. (2007). The IL-6/sIL-6R complex as a novel target for therapeutic approaches. Expert Opin. Ther. Targets *11*, 613–624.

Sahai, E., and Marshall, C.J. (2003). Differing modes of tumour cell invasion have distinct requirements for Rho/ROCK signalling and extracellular proteolysis. Nat. Cell Biol. *5*, 711–719.

Salguero, G., Schuett, H., Jagielska, J., Schley, R., Tallone, E., Luchtefeld, M., Drexler, H., Müller, W., Grote, K., and Schieffer, B. (2009). Hepatocyte gp130 deficiency reduces vascular remodeling after carotid artery ligation. Hypertension *54*, 1035–1042.

Sanz-Moreno, V., Gadea, G., Ahn, J., Paterson, H., Marra, P., Pinner, S., Sahai, E., and Marshall, C.J. (2008). Rac activation and inactivation control plasticity of tumor cell movement. Cell *135*, 510–523.

Snyder, M., Huang, X.Y., and Zhang, J.J. (2008). Identification of novel direct Stat3 target genes for control of growth and differentiation. J. Biol. Chem. *283*, 3791–3798.

Song, Y., Qian, L., Song, S., Chen, L., Zhang, Y., Yuan, G., Zhang, H., Xia, Q., Hu, M., Yu, M., et al. (2008). Fra-1 and Stat3 synergistically regulate activation of human MMP-9 gene. Mol. Immunol. *45*, 137–143.

Straight, A.F., Cheung, A., Limouze, J., Chen, I., Westwood, N.J., Sellers, J.R., and Mitchison, T.J. (2003). Dissecting temporal and spatial control of cytokinesis with a myosin II Inhibitor. Science *299*, 1743–1747.

Thompson, J.E., Cubbon, R.M., Cummings, R.T., Wicker, L.S., Frankshun, R., Cunningham, B.R., Cameron, P.M., Meinke, P.T., Liverton, N., Weng, Y., and DeMartino, J.A. (2002). Photochemical preparation of a pyridone containing tetracycle: a Jak protein kinase inhibitor. Bioorg. Med. Chem. Lett. *12*, 1219–1223.

van Kempen, L.C., Ruiter, D.J., van Muijen, G.N., and Coussens, L.M. (2003). The tumor microenvironment: a critical determinant of neoplastic evolution. Eur. J. Cell Biol. *82*, 539–548.

Viros, A., Fridlyand, J., Bauer, J., Lasithiotakis, K., Garbe, C., Pinkel, D., and Bastian, B.C. (2008). Improving melanoma classification by integrating genetic and morphologic features. PLoS Med. *5*, e120.

Wilkinson, S., Paterson, H.F., and Marshall, C.J. (2005). Cdc42-MRCK and Rho-ROCK signalling cooperate in myosin phosphorylation and cell invasion. Nat. Cell Biol. *7*, 255–261.

Wolf, K., Mazo, I., Leung, H., Engelke, K., von Andrian, U.H., Deryugina, E.I., Strongin, A.Y., Bröcker, E.B., and Friedl, P. (2003). Compensation mechanism in tumor cell migration: mesenchymal-amoeboid transition after blocking of pericellular proteolysis. J. Cell Biol. *160*, 267–277.

Wyckoff, J.B., Pinner, S.E., Gschmeissner, S., Condeelis, J.S., and Sahai, E. (2006). ROCK- and myosin-dependent matrix deformation enables protease-independent tumor-cell invasion in vivo. Curr. Biol. *16*, 1515–1523.

Xie, T.X., Wei, D., Liu, M., Gao, A.C., Ali-Osman, F., Sawaya, R., and Huang, S. (2004). Stat3 activation regulates the expression of matrix metalloproteinase-2 and tumor invasion and metastasis. Oncogene *23*, 3550–3560.

Xiong, H., Zhang, Z.G., Tian, X.Q., Sun, D.F., Liang, Q.C., Zhang, Y.J., Lu, R., Chen, Y.X., and Fang, J.Y. (2008). Inhibition of JAK1, 2/STAT3 signaling induces apoptosis, cell cycle arrest, and reduces tumor cell invasion in colorectal cancer cells. Neoplasia *10*, 287–297.

Yakata, Y., Nakayama, T., Yoshizaki, A., Kusaba, T., Inoue, K., and Sekine, I. (2007). Expression of p-STAT3 in human gastric carcinoma: significant correlation in tumour invasion and prognosis. Int. J. Oncol. *30*, 437–442.

Yamaoka, K., Saharinen, P., Pesu, M., Holt, V.E., 3rd, Silvennoinen, O., and O'Shea, J.J. (2004). The Janus kinases (Jaks). Genome Biol. *5*, 253.

Yu, H., Pardoll, D., and Jove, R. (2009). STATs in cancer inflammation and immunity: a leading role for STAT3. Nat. Rev. Cancer *9*, 798–809.

Yue, P., and Turkson, J. (2009). Targeting STAT3 in cancer: how successful are we? Expert Opin. Investig. Drugs *18*, 45–56.

Zhao, S., Venkatasubbarao, K., Lazor, J.W., Sperry, J., Jin, C., Cao, L., and Freeman, J.W. (2008). Inhibition of STAT3 Tyr705 phosphorylation by Smad4 suppresses transforming growth factor beta-mediated invasion and metastasis in pancreatic cancer cells. Cancer Res. *68*, 4221–4228.